Author(s): Auranen, Kalle; Uusitalo, Juha; Juutinen, Sakari; Jakobsson, Ulrika; Grahn, Tuomas; Greenlees, Paul; Hauschild, Karl; Herzan, Andrej; Julin, Rauno; Konki, Joonas; Leino, Matti; Pakarinen, Janne; Partanen, Jari; Peura, Pauli; Rahkila, Panu; Ruotsalainen, Panu; Sandzelius, Mikael; Sarén, Jan; Scholey, Catherine; Sorri, Juha; Stolze, Sanna

Title: Spectroscopy of At 201 including the observation of a shears band and the 29/2 + isomeric state

Year: 2015

Version:

Please cite the original version:

Auranen, K., Uusitalo, J., Juutinen, S., Jakobsson, U., Grahn, T., Greenlees, P., Hauschild, K., Herzan, A., Julin, R., Konki, J., Leino, M., Pakarinen, J., Partanen, J., Peura, P., Rahkila, P., Ruotsalainen, P., Sandzelius, M., Sarén, J., Scholey, C., . . . Stolze, S. (2015). Spectroscopy of At 201 including the observation of a shears band and the 29/2 + isomeric state. Physical Review C, 91(2), Article 024324. https://doi.org/10.1103/PhysRevC.91.024324

Spectroscopy of ^{201}At including the observation of a shears band and the $29/2^+$ isomeric state

K. Auranen,[1,*] J. Uusitalo,[1] S. Juutinen,[1] U. Jakobsson,[1,†] T. Grahn,[1] P. T. Greenlees,[1] K. Hauschild,[2] A. Herzáň,[1] R. Julin,[1] J. Konki,[1] M. Leino,[1] J. Pakarinen,[1] J. Partanen,[1] P. Peura,[1] P. Rahkila,[1] P. Ruotsalainen,[1] M. Sandzelius,[1] J. Sarén,[1] C. Scholey,[1] J. Sorri,[1] and S. Stolze[1]

[1]*University of Jyvaskyla, Department of Physics, P. O. Box 35, FI-40014 University of Jyvaskyla, Finland*

[2]*CSNSM, IN2P3-CNRS, F-91405 Orsay Campus, France*

(Received 18 December 2014; published 24 February 2015)

The excited states of ^{201}At were studied and an isomeric $^{29}/_{2}^{+}$ state [$T_{1/2} = 3.39(9)$ μs] was identified by using a fusion-evaporation reaction, a gas-filled recoil separator, and recoil gating techniques. The $^{29}/_{2}^{+}$ state is suggested to originate from the $\pi(h_{9/2}) \otimes |^{200}\mathrm{Po};11^{-}\rangle$ configuration, and it decays through the 269- and 339-keV $E2$- and $E3$-type transitions, respectively. Moreover, a cascade of magnetic dipole transitions that is suggested to originate from a shears band was observed by using recoil-gated $\gamma - \gamma(-\gamma)$ coincidence techniques.

DOI: 10.1103/PhysRevC.91.024324 PACS number(s): 23.20.Lv, 23.20.Nx, 23.35.+g, 27.80.+w

I. INTRODUCTION

The region of neutron deficient nuclei around lead offers a large variety of interesting nuclear phenomena. These phenomena include, for example, coexisting different nuclear shapes, sudden changes in the the ground-state deformation, and changes in the ground-state spin and parity between neighboring nuclei. In neutron-deficient even-mass polonium nuclei, spherical or nearly spherical shapes can be found near the $N = 126$ shell closure. When moving from the shell closure towards the proton dripline there is a change from spherical structures to oblate deformed, and onward to prolate deformed, collective structures close to the neutron midshell $N = 104$ (see, for example, Refs. [1–5]). Similar behavior can be anticipated for astatine nuclei, since they can be described as an odd proton coupled to the polonium core.

To date only a little is known for the excited states of the ^{201}At. In the experiment performed by Dybdal *et al.* [6] eight γ-ray transitions associated to ^{201}At were identified. Four of these transitions form a negative-parity cascade up to tentative spin of $^{23}/_{2}^{-}$, and other four transitions were assigned to a positive-parity cascade. The level schemes of the neighboring astatine nuclei are known with much more detail (see, for example, Refs. [6–8]). In addition, several isomeric states have been identified in the neighboring astatine nuclei, hence a more detailed study of ^{201}At is needed.

The $^{29}/_{2}^{+}$ isomeric state has been observed previously in the astatine isotopes ^{199,205,209,211}At [7–10]. These observations are consistent, but a lack of data exists concerning the $^{29}/_{2}^{+}$ state in isotopes ^{197,201,203,207}At. In ^{197,199}At a strongly coupled rotational band is observed to feed the $^{13}/_{2}^{+}$ isomeric state [7]. However, in ^{203}At the rotational structure vanishes [6]. The existing data for the intermediate nucleus ^{201}At are scarce, hence the existence of the rotational structure remains as an open question. In ^{195}At and lighter isotopes the intruder $^{1}/_{2}^{+}$ state becomes the ground state, and therefore the whole excitation scheme changes drastically [11,12].

At the beginning of the 1990s rotational-like cascades of $M1$-type transitions were found in nearly spherical nuclei. One of the first examples was found in ^{199}Pb. The regularity of the γ-ray spectra of these cascades was astonishing, almost like a superdeformed band. To date, over 50 such bands have been found mainly in $^{191-202}$Pb and $^{198-203}$Bi [13]. Only a few examples are known in nuclei heavier than bismuth, these are ^{205}Rn [14], ^{204}At, and ^{206}Fr [15]. In addition, some examples from other mass regions are known, for example, in cadmium [16], tin [17,18], and samarium [19] nuclei. These so-called shears bands can be explained with the tilted-axis cranking model [20].

The present work aims to fill a gap in the systematics of the $^{29}/_{2}^{+}$ isomeric state and improve the knowledge of the excited states in ^{201}At. In this article the deexcitation, half-life, and feeding of the $^{29}/_{2}^{+}$ isomeric state will be presented along with a significantly extended level scheme, including a shears band.

II. EXPERIMENTAL DETAILS

The experiment was performed in the Accelerator Laboratory at the Department of Physics at the University of Jyväskylä. The astatine nuclei of interest were produced using the fusion-evaporation reaction ^{165}Ho(^{40}Ar,$4n$)^{201}At. Production yields for the nuclei produced in this experiment can be estimated from the α-particle energy spectrum shown in Fig. 1. The self-supporting holmium target had a thickness of 350 μg/cm^2. The $^{40}Ar^{8+}$ beam was produced using an electron cyclotron resonance ion source and was accelerated with the K-130 cyclotron to an energy of 172 MeV. Moreover, a typical intensity of 11 pnA (particle nA) and an irradiation time of 83 h were used for the production of ^{201}At.

The JUROGAM II array consisting of Compton-suppressed high-purity germanium detectors (HPGe) was used to detect prompt γ rays at the target position. The array consists of 24 clover [21] and altogether 15 Phase1- [22] and GASP- [23] type detectors. The gas-filled recoil separator RITU [24,25] was used to separate the fusion-evaporation residues (later recoils) from the primary beam and other unwanted particles. The recoils were then guided through a multiwire proportional

*kalle.auranen@jyu.fi

†Present address: Department of Physics, Royal Institute of Technology, SE-10691 Stockholm, Sweden.

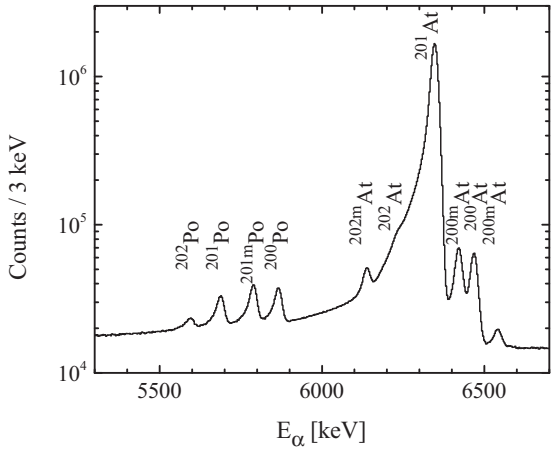

FIG. 1. Raw α-particle energy spectrum observed in the DSSD obtained with the reaction used in this study.

gas counter (MWPC) to the focal plane of RITU, where they were studied using the GREAT spectrometer [26]. In GREAT the recoils were implanted into a 300-μm-thick double-sided silicon strip detector (DSSD) surrounded by 28 silicon PIN diodes in a box arrangement. The delayed γ rays at the focal plane were detected with three clover detectors and one planar-type HPGe detector placed in close geometry around the DSSD. An add-back procedure was introduced to the analysis of all γ-ray data observed in clover-type detectors. Data from all channels were recorded independently using the triggerless total data readout (TDR) method [27]. Absolute time stamps for each event were given by a 100-MHz clock. The data analysis was performed using GRAIN [28] software. A more detailed description of the experimental setup is presented in Ref. [29].

III. RESULTS

A. $^{29}/_{2}^{+}$ isomeric state

Figure 2(a) shows the recoil-gated prompt γ-ray singles energy spectrum observed in JUROGAM II. Figure 2(b) shows the delayed γ-ray energy spectrum observed in the focal-plane clover array within 14 μs from the recoil implantation. This search time corresponds roughly to 4 times the half-life of the isomeric state under interest, and it is applied to the analysis of all delayed γ-ray spectra presented in this work. The deduction of the half-life is explained at the end of this section. When comparing these two spectra, two observations can be made: First, the same γ-ray transitions can be identified in both spectra, and some of these are previously known [6]. Second, the 269- and 339-keV transitions are present only in the delayed spectrum. These two observations suggest that there is a high-lying isomeric state in ^{201}At, which is depopulated by the 269- and 339-keV transitions.

Figure 3 shows some examples of the γ-γ coincidence analysis of the focal-plane clover data. In Fig. 3(a) the energy spectrum of γ rays in prompt coincidence with the 269-keV transition is shown. In Fig. 3(b) a prompt coincidence with the 476-keV or the 594-keV γ-ray transition is demanded. The

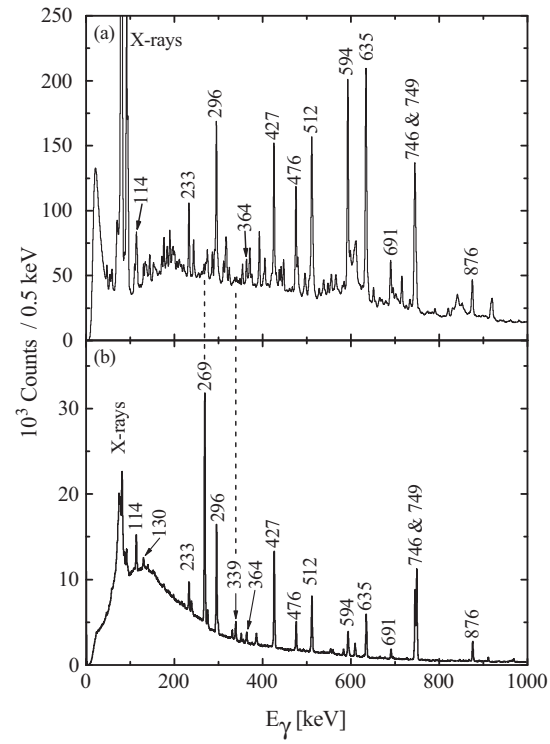

FIG. 2. (a) Recoil-gated γ-ray energy spectrum observed in JUROGAM II. (b) γ-Ray energy spectrum observed in the focal-plane clover array within 14 μs from the recoil implantation.

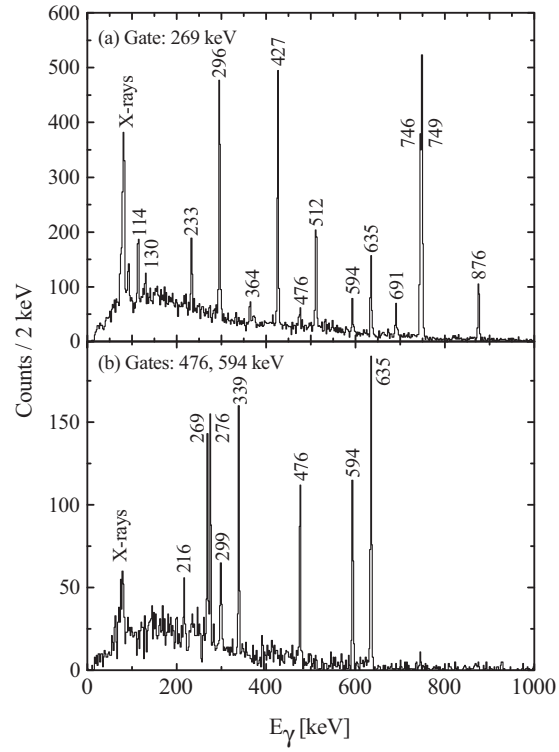

FIG. 3. Recoil-gated delayed γ-γ energy spectra observed in the focal-plane clover array: (a) Energy spectrum of γ rays in prompt coincidence with the 269-keV γ ray. (b) Energy spectrum of γ rays in prompt coincidence with the 476-keV or the 594-keV γ-ray transition.

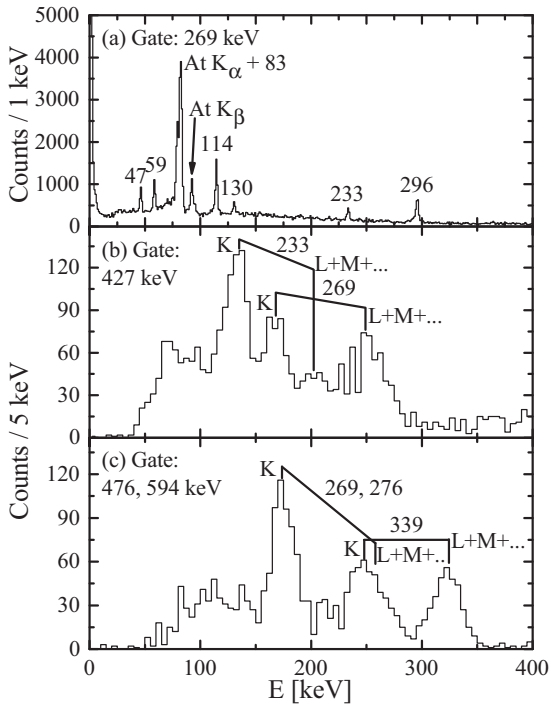

FIG. 4. (a) Recoil-gated delayed low-energy γ-ray energy spectrum observed in the planar detector. Prompt coincidence with the 269-keV γ-ray transition in any of the focal-plane clover detectors was demanded. Conversion electron energy spectra observed in the PIN diodes: (b) conversion electrons in prompt coincidence with the 427-keV γ ray observed in focal-plane clover array. (c) same as in panel (b) but with 476- or 594-keV γ-ray energy gate used.

427-, 746-, and 749-keV transitions are known to belong to the positive-parity cascade in ^{201}At [6]. The spectrum shown in Fig. 3(a) suggests that the 269-keV transition mainly feeds this positive-parity cascade, and, respectively, Fig. 3(b) suggests that the 339-keV transition feeds the negative-parity cascade. The 476-, 594-, and 635-keV transitions were previously assigned to the negative-parity band [6] in ^{201}At.

In addition to the transitions visible in the presented clover spectra, there are a few low-energy transitions that are only observed in the planar detector. Figure 4(a) shows the energy spectrum of low-energy γ rays observed in the planar detector in coincidence with the 269-keV γ ray observed in any of the focal-plane clover detectors. It is worth noting the abnormally high K_α/K_β x-ray intensity ratio. This suggests that there is a γ-ray transition in the positive-parity cascade with a transition energy partially overlapping with the K_α x-ray peak.

Observed γ rays below the isomer are listed in Table I together with the extracted angular distribution parameter A_2, when obtained. The deduction of the multipolarity information from angular distributions with the present experimental setup is explained in Ref. [29]. The level scheme below the isomer was built based on γ-γ coincidence information, multipolarity information, and energy-sum arguments. The validity of the level structure was confirmed with the transition intensities at the focal plane I_{TR}(FP) for each transition, and the obtained level scheme is presented in Fig. 5. Transition

TABLE I. Observed γ rays following the decay of the $^{29}/_{2}^{+}$ isomeric state. I_γ is the relative γ-ray intensity and A_2 is the angular distribution parameter, and both are deduced from JUROGAM II data. The γ-ray energy E_γ and the transition intensity at the focal plane I_{TR}(FP) are deduced from the focal-plane clover data if not specified. Internal-conversion coefficients for the calculation of I_{TR}(FP) were taken from Ref. [30]. I_{TR}(FP) is normalized such that the 269-keV γ-transition has an intensity of 100.

E_γ (keV)	I_γ	A_2	I_{TR} (FP)	I_i^π ($\hbar$)	I_f^π ($\hbar$)
46.5(2)[a]			90(30)[a]	$^{25}/_{2}^{+}$	$^{23}/_{2}^{+}$
58.5(2)[a]			6(2)	$^{13}/_{2}^{+}$	$^{11}/_{2}^{-}$
83.0(4)[b]			120(40)[c]	$^{23}/_{2}^{+}$	$^{21}/_{2}^{+}$
114.1(2)			12(2)	$^{13}/_{2}^{+}$	$^{13}/_{2}^{-}$
130.3(2)	3.9(4)	−0.36(7)	20(3)	$^{17}/_{2}^{+}$	$^{17}/_{2}^{+}$
216.3(3)			1.3(3)	$^{21}/_{2}^{+}$	$^{21}/_{2}^{-}$
233.4(2)	14.5(4)	−0.05(2)	24(3)	$^{17}/_{2}^{+}$	$^{15}/_{2}^{+}$
269.0(2)			118(11)	$^{29}/_{2}^{+}$	$^{25}/_{2}^{+}$
275.5(2)	6.6(2)	−0.47(2)	12(2)	$^{23}/_{2}^{-}$	$^{21}/_{2}^{-}$
295.9(2)	40(2)	0.11(4)	60(6)	$^{21}/_{2}^{+}$	$^{17}/_{2}^{+}$
299.3(2)			5.0(7)	$^{23}/_{2}^{+}$	$^{21}/_{2}^{-}$
339.2(2)			14(2)	$^{29}/_{2}^{+}$	$^{23}/_{2}^{-}$
364.1(3)	6.5(3)	−0.11(3)	8(2)	$^{17}/_{2}^{+}$	$^{15}/_{2}^{+}$
426.5(2)	39(2)	0.14(7)	69(9)	$^{21}/_{2}^{+}$	$^{17}/_{2}^{+}$
476.2(2)	33(1)	0.13(4)	21(4)	$^{21}/_{2}^{-}$	$^{17}/_{2}^{-}$
511.8(2)		−0.14(3)	38(7)[d]	$^{15}/_{2}^{+}$	$^{13}/_{2}^{+}$
593.8(2)	77(3)	0.08(2)	25(4)	$^{17}/_{2}^{-}$	$^{13}/_{2}^{-}$
635.1(2)	100(3)	0.09(4)	42(6)	$^{13}/_{2}^{-}$	$^{9}/_{2}^{-}$
691.1(2)			11(2)	$^{11}/_{2}^{-}$	$^{9}/_{2}^{-}$
745.5(2)	74(2)	0.4(2)	72(8)	$^{17}/_{2}^{+}$	$^{13}/_{2}^{+}$
749.3(2)			105(12)	$^{13}/_{2}^{+}$	$^{9}/_{2}^{-}$
876.1(2)	19.4(6)	0.16(3)	24(3)	$^{17}/_{2}^{+}$	$^{13}/_{2}^{+}$

[a]Deduced from the recoil-gated planar singles spectrum.
[b]Calculated from the assumption that in a closed loop of transitions the energy shift is zero. Two loops were used, the weighted average of the results is presented.
[c]Deduced from the 746- or 749-keV gated planar vs clover γ-γ data. The number of K_α x rays is subtracted based on the number of observed K_β x rays.
[d]Deduced from 296-keV gated focal-plane clover γ-γ data.

intensities are listed in Table I, and the internal conversion coefficients were taken from the BrIcc [30]. Based on the multipolarity information and the I_{TR}(FP) information for each transition, the spin and parity of the isomer is suggested to be $^{29}/_{2}^{+}$.

The isomer decays mainly through the 269-keV $E2$-type transition, but also an $E3$-type transition with a transition energy of 339 keV has been observed. These transition-type assignments were confirmed by the conversion-electron energy spectra observed in the PIN diodes. These spectra are shown in Figs. 4(b) and 4(c). The deduced internal-conversion intensity ratio $K/L+M+\ldots = 0.93(5)$ matches well with the theoretical [30] value of 0.89(2) calculated for the 269-keV $E2$-type transition. The 339-keV K-conversion peak overlaps with the $L + M + \cdots$-conversion peaks from the 269- and 276-keV transitions. Therefore, the number of 269- and 276-keV $L + M + \cdots$-conversion events in the ∼250-keV peak in Fig. 4(c) were estimated. These estimates were based on

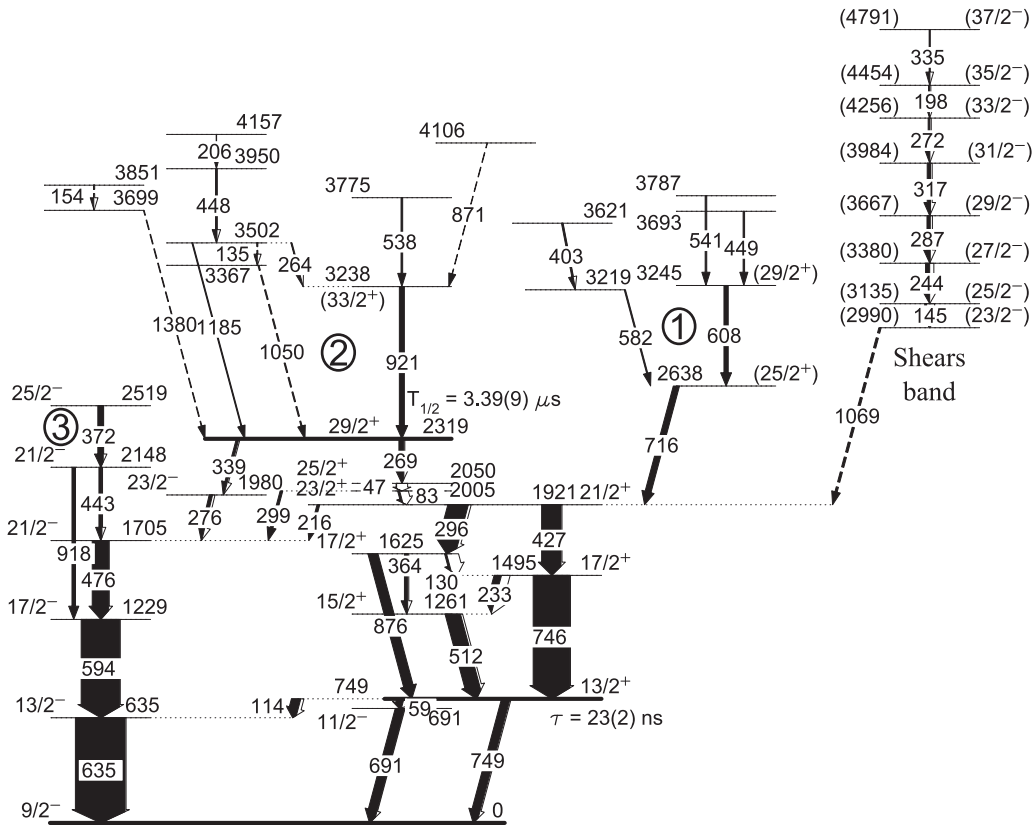

FIG. 5. Partial level scheme of ^{201}At. Levels associated with the isomeric $^{1}/_{2}^{+}$ state [$T_{1/2} = 45(3)$ ms] lying at the excitation energy of 459 keV are shown in Ref. [29]. The number inside a circle indicates the number of a transition group used to categorize transitions. The mean lifetime of the $^{13}/_{2}^{+}$ state is taken from Ref. [6], and the rest of the information is from this work.

the intensity ratio $I_\gamma(269)/I_\gamma(276)$ [extracted from the spectrum shown in Fig. 3(b)], the number of observed 269- and 276-keV K-conversion events, and the theoretical $K/L+M+\ldots$ ratios for the 269-keV $E2$ and 276-keV $M1$ transitions. The remaining events in the ∼250-keV peak belong to the 339-keV K conversion. For the 339-keV transition this method yields the $K/L+M+\ldots$ intensity ratio of 0.45(4), which is in agreement with with the theoretical value of 0.416(8) for a 339-keV $E3$-type transition.

Figure 6 shows the time distribution between the recoil implantation and the following 269-keV γ ray observed in the planar detector. In addition, one of the 296-, 427-, 594-, 635-, 746-, or 749-keV γ rays has been demanded to be observed in any of the focal-plane clover detectors in prompt coincidence with the 269-keV γ ray. The logarithmic time scale method [31] yields a half-life of 3.39(9) μs for the $^{29}/_{2}^{+}$ isomeric state. This half-life corresponds to reduced transition strengths of $1.33(4) \times 10^{-3}$ W.u. and 11(2) W.u. for the 269-keV $E2$- and the 339-keV $E3$-type transitions, respectively.

B. Shears band

Figure 7 shows the low-energy part of the double-gated prompt γ-ray energy spectrum. The other gate is a sum of gates 145, 198, 244, 272, 287, 317, and 335 keV, and the other is the sum of gates 427 and 746 keV. In the spectrum there are a number of low-energy $M1$ transitions. This transition-type assignment is supported by the stretched dipolelike angular distributions, and high x-ray yield in coincidence with these transitions. In Fig. 7 these $M1$ transitions are labeled with

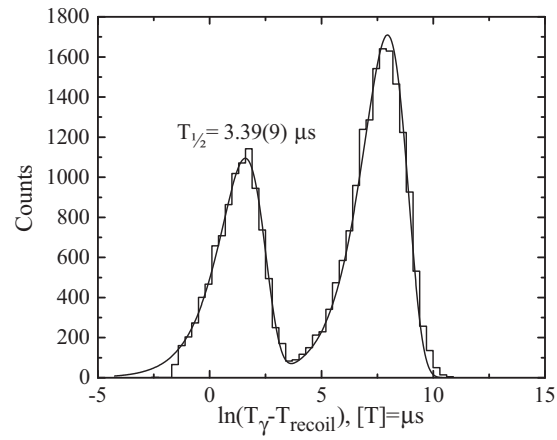

FIG. 6. Time distribution between the recoil implantation and the subsequent 269-keV γ-ray transition observed in the planar detector. Prompt coincidence with a 296-, 427-, 594-, 635-, 746-, or 749-keV γ ray in any of the focal-plane clovers is demanded. The logarithmic time scale method [31] yields a half-life of 3.39(9) μs. The longer living component of the distribution is a result from random γ-ray coincidences, originating, for example, from Compton scattering.

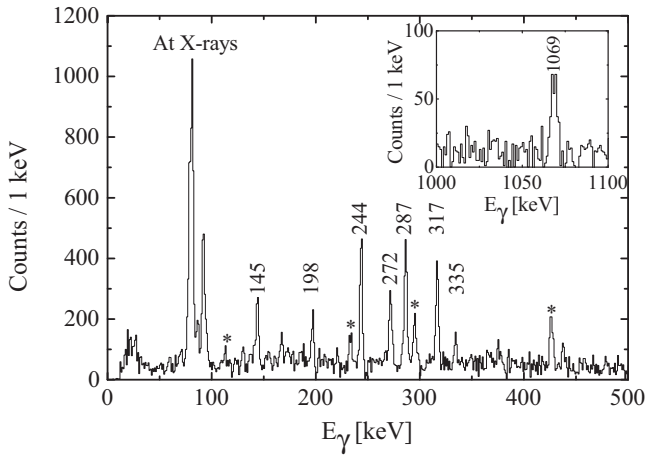

FIG. 7. Recoil-gated prompt γ-ray transitions in coincidence with either the 427- or 746-keV transitions and any of the low-energy transitions listed in Table II. Transitions labeled with energy are suggested to belong to the shears band. Transitions marked with an asterisk are known to belong to the positive-parity cascade. The inset shows the high-energy part of the spectrum.

energy, and they are listed in Table II. In principle, there could also be weak $E2$-type crossover transitions, but these were not observed. The lower limits for the $^{B(M1)}/_{B(E2)}$ ratios in Table II were estimated by integrating the area of the smallest observable peak near the energy of the unobserved $E2$ transition. Based on the γ-γ- and γ-γ-γ -coincidence analysis, the $M1$ transitions form a cascade. This cascade is suggested to form a shears band, see the discussion in the Sec. IV B. The shears band is also shown in Fig. 5. In coincidence with these transitions there is a 1069-keV dipole transition. This transition, and the transitions in the proposed shears band, are in coincidence with the 296- and 427-keV transitions but not with the 83-keV transition. Based on these arguments the shears band is proposed to decay through the 1069-keV transition to the $^{21}/_{2}^{+}$ state. Magnetic or electric character of this transition cannot be distinguished with the information obtained in this study. For the parity assignment of the shears band, see the discussion section. In addition, the total transition intensity of the 145-keV transition is much higher than the 1069-keV transition intensity. Therefore there must be at least one additional, unobserved decay path.

TABLE II. γ-ray transitions associated with the shears band. I_γ normalized such that $I_\gamma(635\text{keV}) = 100$. Intensities and energies are deduced from the sum of gates gates (746- and 427-keV transitions) γ-γ data.

E_γ (keV)	I_γ	A_2	I_i^π ($\hbar$)	I_f^π ($\hbar$)	$^{B(M1)}/_{B(E2)}$ (μ_N^2/e^2b^2)
145.0(4)	3.7(3)	−0.5(2)	$(^{25}/_{2}^{-})$	$(^{23}/_{2}^{-})$	—
197.9(4)	1.6(2)	−0.80(12)	$(^{33}/_{2}^{-})$	$(^{31}/_{2}^{-})$	>8
244.4(4)	8.3(5)	−0.59(9)	$(^{27}/_{2}^{-})$	$(^{25}/_{2}^{-})$	>30
272.3(4)	3.5(3)	−0.45(11)	$(^{35}/_{2}^{-})$	$(^{33}/_{2}^{-})$	>35
286.9(4)	6.6(4)	−0.47(3)	$(^{29}/_{2}^{-})$	$(^{27}/_{2}^{-})$	>25
317.3(4)	6.7(4)	−0.81(9)	$(^{31}/_{2}^{-})$	$(^{29}/_{2}^{-})$	>30
335.0(4)	1.5(2)	−0.66(4)	$(^{37}/_{2}^{-})$	$(^{35}/_{2}^{-})$	>2
1068.9(4)	4.5(3)	−0.47(5)	$(^{23}/_{2}^{-})$	$^{21}/_{2}^{+}$	

C. Other observed transitions

There are a large number of transitions in addition to those in the shears band and those below the $^{29}/_{2}^{+}$ isomeric state. These transitions can be divided into three groups. Groups 1 and 2 consist of the transitions feeding the $^{21}/_{2}^{+}$ and the $^{29}/_{2}^{+}$ states, respectively. Group 3 is formed by the transitions associated with the negative-parity ground-state cascade. Figures 8(a) and 8(b) show most of the transitions belonging to groups 1 and 2, respectively. In Fig. 8(a) the transitions in coincidence with the 716-keV transition are shown. The transitions connected with dashed lines form together, with the 716-keV transition, group 1. Figure 8(b) shows the γ-ray singles spectrum where the recoil has been isomer tagged with a 269-, 427-, 635-, 746-, or 749-keV delayed γ-ray transition observed in the focal-plane clover array within 14 μs from the recoil implantation. The transitions labeled with energy in Fig. 8(b) are those which feed the $^{29}/_{2}^{+}$ isomeric state. The transitions belonging to groups 1–3 are listed in Table III. The level scheme of these groups were constructed based on the γ-γ(-γ) coincidence information, the transition

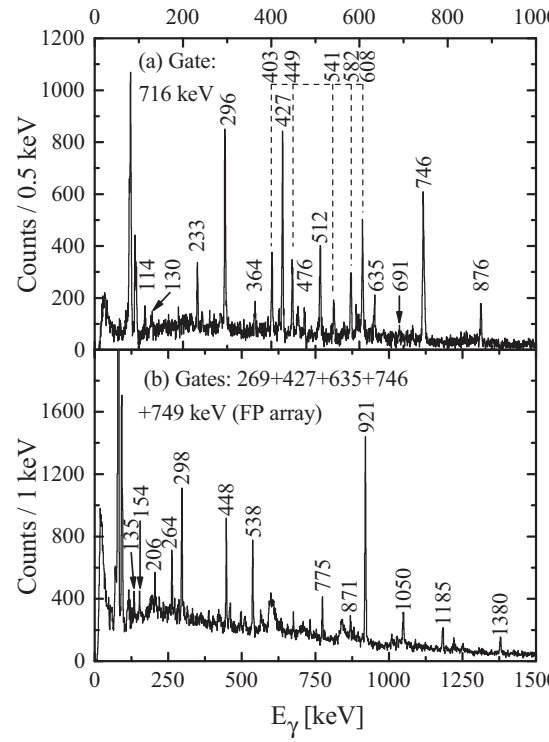

FIG. 8. Prompt γ-ray transitions observed in JUROGAM II: In panel (a) transitions in coincidence with the 716-keV transition are shown. Transitions connected with a dashed line belong to group 1 together with the 716-keV transition. Panel (b) shows the singles γ-ray spectrum in delayed coincidence with any of the most intense γ-ray transitions (observed in the focal-plane clover array) below the $^{29}/_{2}^{+}$ isomeric state. Note the different energy scales in panels (a) and (b).

TABLE III. Remaining observed γ-ray transitions. Information for the group 1 transitions is obtained from the sum-gated (296- and 427-keV transitions) γ-γ data. Information for group 2 is obtained from the 269-, 427-, 635-, 749-, or 749-keV delayed γ-ray tagged singles spectrum. The group 3 information is obtained from recoil-gated singles data. I_γ normalized such that $I_\gamma(635\ \text{keV}) = 100$.

Group	E_γ (keV)	I_γ	A_2	I_i^π ($\hbar$)	I_f^π ($\hbar$)
1	402.6(4)	2.6(3)	−0.7(2)		
1	448.5(4)	2.8(2)	−0.4(2)		
1	540.5(5)	3.1(3)			
1	581.6(4)	2.1(2)	−0.44(7)		
1	607.8(4)	8.4(8)	0.35(8)	$(^{29}/_2{}^+)$	$(^{25}/_2{}^+)$
1	716.3(4)	11.9(7)	0.46(4)	$(^{25}/_2{}^+)$	$^{21}/_2{}^+$
2	135.0(4)	0.50(4)			
2	153.6(4)	0.47(4)			
2	206.2(4)	0.31(5)			
2	263.6(4)	1.2(2)	−0.26(9)		
2	297.5(4)[a]	3.0(2)			
2	448.4(4)	2.9(2)	−0.3(2)		
2	538.2(4)	2.9(2)			
2	774.9(4)[a]	1.7(2)	0.29(4)		
2	870.5(4)	0.93(8)			
2	921.1(4)	10.1(6)	0.20(3)	$(^{33}/_2{}^+)$	$^{29}/_2{}^+$
2	1049.9(4)	2.2(2)	−0.7(3)		
2	1184.5(4)	1.7(2)	0.40(8)		
2	1379.9(5)	1.4(2)			
3	371.7(4)	10.9(4)	0.16(6)	$^{25}/_2{}^-$	$^{21}/_2{}^-$
3	442.6(4)	6.0(2)	0.35(8)	$^{21}/_2{}^-$	$^{21}/_2{}^-$
3	917.8(4)	7.0(4)	0.37(6)	$^{21}/_2{}^-$	$^{17}/_2{}^-$

[a]Transition is not placed in the level scheme, as it is not in coincidence with other transitions in group 2. However, this transition is probably feeding the $^{29}/_2{}^+$ state.

intensity balance, and energy-sum arguments. The obtained level scheme are shown in Fig. 5.

IV. DISCUSSION

A. The $^{29}/_2{}^+$ isomeric state and related levels

Figure 9(a) shows the systematics of several negative-parity states observed in At nuclei compared to the lowest yrast states of their isotonic polonium partners. It is evident that the energy of the observed negative-parity states up to the $^{21}/_2{}^-$ state follow the energies of the yrast states in their even-even Po isotones. These findings support the earlier [6] interpretation that these negative-parity states in ^{201}At originate from the weak coupling of an $h_{9/2}$ proton to the polonium core. This interpretation is also suggested for the neighboring isotopes ^{199}At [7], ^{203}At [6], and ^{205}At [39]. In ^{197}At the deviation of the level spacing is interpreted to originate from the strengthening of the odd proton coupling to the core [7]. In ^{195}At and lighter isotopes [11,12] the $^1/_2{}^+$ intruder state originating from the $\pi(s_{1/2})^{-1}$ configuration becomes the ground state. Hence the scheme of observed excited states changes drastically. Also in the nearby francium nuclei ^{203}Fr (isotone of ^{201}At) and ^{205}Fr (^{201}At + α) the negative-parity states have been suggested to originate from the coupling of an $h_{9/2}$ proton to the radon core, see Refs. [40,41].

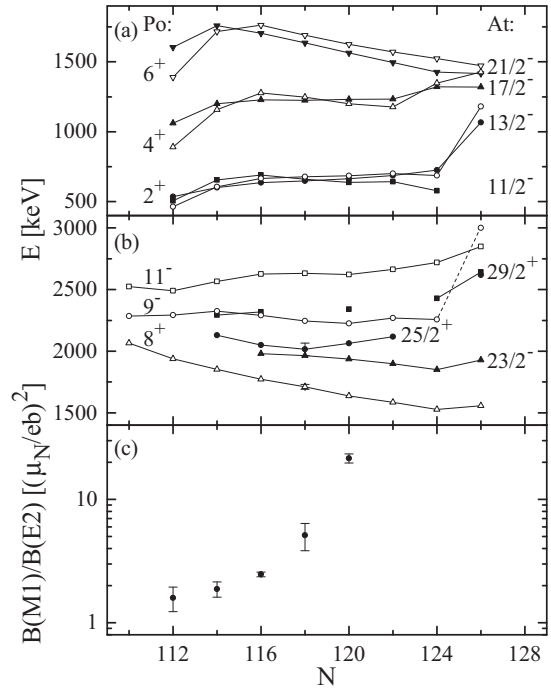

FIG. 9. Energy systematics of selected astatine (solid symbols) and polonium (open symbols) levels: In panel (a) negative-parity levels in the astatines are compared to the yrast levels of the polonium isotones. In panel (b) the level energies of the $^{29}/_2{}^+$, $^{25}/_2{}^+$, and $^{23}/_2{}^-$ states are compared with the 11^-, 9^-, and 8^+ states in corresponding polonium isotonic partners. The data points with the error bars are floating in the level scheme. The error bars correspond to the maximum of estimated floating. In panel (c) the measured $^{B(M1)}/_{B(E2)}$ ratios for the decay of the lowest $^{17}/_2{}^+$ state in the odd mass astatine isotopes $^{197-205}$At are shown. Data for all panels are taken from Refs. [4,6–10,32–38] and the present work. Neutron number of ^{201}At is 116.

In addition to the isomeric 11^- [2596 keV, $\pi(h_{9/2}i_{13/2})$] state, also the 9^- [2261 keV, $\nu(f_{5/2}^{-1}i_{13/2}^{-1})$], 8^- (2237 keV), 7^- [2136 keV, $\nu(f_{5/2}^{-1}i_{13/2}^{-1})$], 5^- [1811 keV, $\nu(f_{5/2}^{-1}i_{13/2}^{-1})$], and 8^+ [1774 keV, $\pi(h_{9/2}^2)$] states have been observed in ^{200}Po, which is the isotonic partner of ^{201}At. Also second [$\sim$2200 keV, $\pi(h_{9/2}f_{7/2})$] and third [2716 keV, $\nu(i_{13/2}^{-2})$] 8^+ states can be expected to exist [42,43]. The 11^- isomeric state decays to the 9^- and 8^+ states via $E2$- and $E3$-type transitions, respectively. In Fig. 9(b) the energy of selected polonium states are compared with the $^{29}/_2{}^+$, $^{25}/_2{}^+$, and $^{23}/_2{}^-$ states energies observed in At nuclei. From the figure one can see that the level energy of the $^{29}/_2{}^+$ state follows the level energy of the isomeric 11^- state in Po nuclei. Also the $^{25}/_2{}^+$ and $^{23}/_2{}^-$ states follow the 9^- and 8^+ states, respectively. Based on these similarities, we propose that the observed isomeric and the subsequent states in ^{201}At result from the coupling of the odd proton to the respective state in the polonium isotone. These configurations are summarized in Table IV, and they are identical to those states that have been suggested earlier in neighboring astatine nuclei [6–8].

TABLE IV. Suggested configurations for some of the observed excited states in ^{201}At.

E (keV)	I ($\hbar$)	Configuration
635	$13/2^-$	$\pi(h_{9/2})\otimes\|^{200}\mathrm{Po};2^+\rangle$
691	$11/2^-$	$\pi(h_{9/2})\otimes\|^{200}\mathrm{Po};2^+\rangle$
749	$13/2^+$	$\pi(i_{13/2})\otimes\pi(h_{9/2})^2_{0+}$
1229	$17/2^-$	$\pi(h_{9/2})\otimes\|^{200}\mathrm{Po};4^+\rangle$
1495	$17/2^+$	$\pi(i_{13/2})\otimes\pi(h_{9/2})^2_{2+}$
1705	$21/2^-$	$\pi(h_{9/2})\otimes\|^{200}\mathrm{Po};6^+\rangle$
1625	$17/2^+$	$\pi(h_{9/2})\otimes\|^{200}\mathrm{Po};5^-\rangle$
1980	$23/2^-$	$\pi(f_{7/2})\otimes\|^{200}\mathrm{Po};8^+_1\rangle$
1921	$21/2^+$	$\pi(h_{9/2})\otimes\|^{200}\mathrm{Po};7^-\rangle$
2005	$23/2^+$	$\pi(h_{9/2})\otimes\|^{200}\mathrm{Po};8^-\rangle$
2050	$25/2^+$	$\pi(h_{9/2})\otimes\|^{200}\mathrm{Po};9^-\rangle$
2148	$21/2^-$	$\pi(f_{7/2})\otimes\|^{200}\mathrm{Po};8^+_2\rangle$
2319	$29/2^+$	$\pi(h_{9/2})\otimes\|^{200}\mathrm{Po};11^-\rangle$
2519	$25/2^-$	$\pi(h_{9/2})\otimes\|^{200}\mathrm{Po};8^+_3\rangle$

The observed isomeric $29/2^+$ state decays through the 269-keV $E2$- and 339-keV $E3$-type transitions. These two transitions have reduced transition strengths of $1.33(4)\times10^{-3}$ W.u. and 11(2) W.u., respectively. Suppression of the $E2$-type transition is understandable, as it requires a significant change of $\pi(h^2_{9/2}i_{13/2})\rightarrow\pi(h_{9/2})\nu(f^{-1}_{5/2}i^{-1}_{13/2})$ in the single-particle configuration. Structural changes in the $\pi(h^2_{9/2}i_{13/2})\rightarrow\pi(h^2_{9/2}f_{7/2})$ $E3$-type transition are much simpler and it involves octupole correlations [44], hence it is favored. The same isomeric state has been observed in ^{199}At [7], ^{205}At [8], ^{209}At [9], and ^{211}At [10]. In ^{199}At only the $E2$ transition (0.044 W.u.) has been observed to depopulate the isomeric state. In ^{205}At both transitions have been observed with reduced transition strengths of $1.8(5)\times10^{-4}$ W.u. and 19(1) W.u. for the $E2$- and $E3$-type transitions, respectively. In ^{209}At and ^{211}At only the $E3$ transition has been observed with transitions strengths of 24(2) W.u. and 16 W.u., respectively [8]. Hence the measured reduced transition strengths in ^{201}At are comparable with the corresponding values in neighboring nuclei. The measured transition strength in the ^{201}At for the $E3$-type transition is comparable with the value of ∼12 W.u. [42] for the $E3$-type transition ($11^-\rightarrow8^+$) in ^{200}Po. Also the $11^-\rightarrow9^-$ $E2$-type transition is strongly hindered (10^{-2} W.u., Ref. [42]) in ^{200}Po.

From Fig. 9(b) one can also observe that the transition energy for the $E3$-type transition decreases as the neutron number decreases. The $E2$-type transition energy stays rather constant. As a result, the deexitation of the $29/2^+$ isomeric state favors the $E2$-type transition in lighter and $E3$-type transition in the heavier astatine isotopes. The favoring of $E2$-type transition can also be seen as an enhancement of the reduced transition strength of the $E2$-type transition when the neutron number decreases, as mentioned above.

The $25/2^+$ states have been reported to have a mean lifetime of 156(3), 98(2), and 17(2) ns in the isotopes ^{207,205,203}At, respectively [6,8,32]. If the lifetime of the $25/2^+$ state develops as might be expected as the neutron number decreases, it should be much shorter than ∼20 ns in ^{201}At. However, the experimental setup (10-ns time resolution) used in this study is not sensitive for lifetimes this short. An effort was made to extract the lifetime of the $13/2^+$ state (23(2) ns, [6]), resulting in a time distribution yielding a lifetime of ∼20 ns. Similar analysis was made to extract the lifetime of the $25/2^+$ state; however, the result was a promptlike time distribution. Hence, based on the data obtained in this study, it can be only deduced that the lifetime of the $25/2^+$ state is much shorter than ∼20 ns.

The $13/2^+$ state in astatine nuclei $^{197-205}$At is suggested to originate from the $\pi(i_{13/2})$ configuration [6–8]. In isotopes ^{197,199}At the $13/2^+$ level is fed by a strongly coupled rotational band, and the $13/2^+$ state is suggested to have an oblate deformation [7,35]. However, in ^{201}At only the levels up to the lowest $17/2^+$ state show this rotational-like behavior. In the excited states higher than this, the rotational structure vanishes. Figure 9(c) shows the $B(M1)/B(E2)$ ratios for the decay of the lowest $17/2^+$ state in $^{197-205}$At. In isotopes lighter than ^{201}At the ratio is small and rather constant. Starting from ^{201}At the ratio grows rapidly as the neutron number increases. This together with the disappearance of the rotational band might indicate a decrease of deformation when moving towards heavier astatine isotopes. Hence the $13/2^+$ state in ^{201}At is suggested to be weakly oblate.

The lowest 2^+ state in ^{198}Pb is known to lie at an excitation energy of 1064 keV [45]. This energy is comparable to the transition energies that feed the $29/2^+$ isomeric state (group 2). Hence the states feeding the $29/2^+$ state might have a $\pi(h^2_{9/2}i_{13/2})\otimes|^{198}\mathrm{Pb};2^+_1\rangle$-like configuration.

B. Shears band

In shears bands a (high-j) proton and neutron are coupled. The coupling creates a total angular momentum vector that does not lie on any of the principal axes. The angle between proton and neutron spins ($\vec{j}_\pi$, $\vec{j}_\nu$) is called the shears angle, and it is often denoted with the symbol θ. Once the proton and neutron states are known, the shears angle can be given using a semiclassical expression,

$$\cos\theta=\frac{\vec{j}_\nu\cdot\vec{j}_\pi}{|\vec{j}_\nu||\vec{j}_\pi|}=\frac{I(I+1)-j_\nu(j_\nu+1)-j_\pi(j_\pi+1)}{2\sqrt{j_\nu(j_\nu+1)j_\pi(j_\pi+1)}}. \quad (1)$$

When the excitation energy is increased, the shears angle decreases (like closing shears), increasing the spin of the system. Hence the name *shears band*. These shears bands have a few general properties that may be summarized as follows:

(i) The states in the band (away from band crossings) follow the pattern of $E(I)-E_0\propto(I-I_0)^2$, where 0 refers to the band-head state.
(ii) The band is formed from strong $M1$ transitions with weak $E2$ crossovers, typically $B(M1)/B(E2)\gtrsim20\ \mu_N^2/\mathrm{e}^2\mathrm{b}^2$ and $B(M1)\sim2$–$10\ \mu_N^2$.
(iii) The structures have small quadrupole deformation.
(iv) The active orbitals must involve high j values.
(v) The ratio of the dynamic moment of inertia over $B(E2)$ is large, $>100\ \mathrm{MeV}^{-1}(\mathrm{eb})^{-2}$, when compared to well-deformed [$\sim10\ \mathrm{MeV}^{-1}(\mathrm{eb})^{-2}$] or superdeformed [$\sim5\ \mathrm{MeV}^{-1}(\mathrm{eb})^{-2}$] bands.

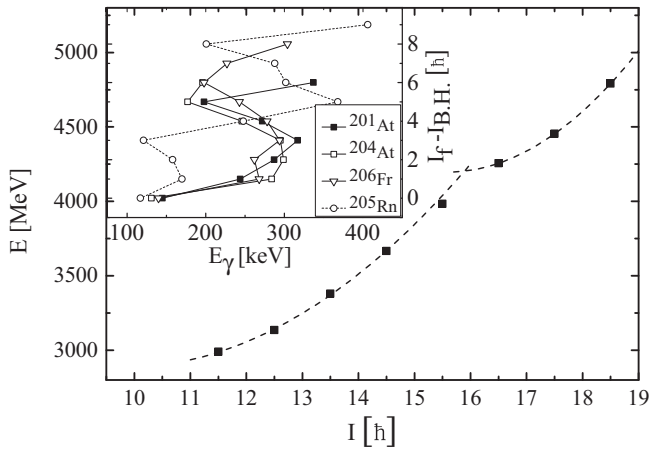

FIG. 10. Energy of the levels in the shears band as a function of the level spin. The spin and excitation energy of the band-head state remain tentative with the information obtained in this study, but any change in the band head will simply move the curve along the vertical or horizontal axis. The dashed lines show two arbitrary parabolas to guide the eye. The inset shows the final-state spin I_f with respect to the band-head spin $I_{\text{B.H.}}$ as a function of the transition energy. Data for ^{204}At and ^{206}Fr are taken from Ref. [15], and for ^{205}Rn from Ref. [14].

Particle-hole coupling is usually needed in order to achieve the large angular momentum of the states in the shears band. Active orbitals must involve high j values in order to allow long sequences of states and transitions between them. Also the deformation of the core must be small enough, otherwise the core rotation dominates over the shears mechanism. Text above is a summary of the annual review publication by Clark and Macchiavelli. For more information, see Ref. [13] and references therein.

The transitions listed in Table II show several properties that are typical for shears bands. Figure 10 shows the energy of the levels in this cascade as a function of the level spin. The spin and excitation energy labeling of the band-head state are tentative, but any change in spin (energy) will only shift the pattern along horizontal (vertical) axis. The dashed lines in Fig. 10 represent two arbitrary parabolas to highlight the parabolic behavior of $E(I)$. This behavior is very typical for the shears band levels away from the band crossings (see property (i) listed above). The bump around spin $\sim 16\hbar$ results from another band crossing the original one. This can also be seen as a "backbending" in the inset of the Fig. 10. The lengths of the shears "blades" may differ before and after the crossing. In the crossing reorienting the shears "blades" by increasing the shears angle produces a state with the same angular momentum at lower energy.

Based on the dipolelike angular distribution of the observed γ rays and x-ray yield, the transitions in the suggested shears band were identified to form a rotational-like cascade of magnetic dipole transitions. In principle, there could also be $E2$-type crossover transitions, but these were not observed. The lack of $E2$ transitions suggests that the reduced transition strength ratio $B(M1)/B(E2)$ for transitions in the observed cascade is large. This can also be seen from the estimated lower limits for the $B(M1)/B(E2)$ ratio shown in Table II. Large $B(M1)/B(E2)$ ratios is again one of the characteristic properties for shears bands (see listed property number (ii)). However, the experimental setup did not allow the absolute measurement of $B(M1)$ or $B(E2)$ values.

TABLE V. Calculated band-head state spin $I_{\text{B.H.}}$ and the maximum spin I_{MAX}, as a function of different proton and neutron configurations for the shears band in ^{201}At. Last column shows the sum of the proton- and neutron-state level energies. Proton-state energies are taken from this work, neutron-state energies are taken from Refs. [42,43]. Experimental band-head state spin is $^{23}/_{2}\ \hbar$ and it lies at the energy of 2990 keV. The observed band crossing takes place at the energy of ~4200 keV and spin $\sim 16\hbar$.

$\lvert\pi\rangle$	$\lvert\nu\rangle$	$I_{\text{B.H.}}$ [$\hbar$]	I_{MAX} [$\hbar$]	$E_\pi + E_\nu$ (keV)
$\lvert i_{13/2}; {}^{13}/_{2}^{+}\rangle$	$\lvert f_{5/2}^{-1} i_{13/2}^{-1}; 7^{-}\rangle$	9.7	14.0	2885
$\lvert i_{13/2}; {}^{13}/_{2}^{+}\rangle$	$\lvert f_{5/2}^{-1} i_{13/2}^{-1}; 8^{-}\rangle$	10.5	15.0	2986
$\lvert i_{13/2}; {}^{13}/_{2}^{+}\rangle$	$\lvert f_{5/2}^{-1} i_{13/2}^{-1}; 9^{-}\rangle$	11.3	16.0	3010
$\lvert (h_{9/2})^2 i_{13/2}; {}^{29}/_{2}^{+}\rangle$	$\lvert f_{5/2}^{-1} i_{13/2}^{-1}; 5^{-}\rangle$	15.5	20.0	4130
$\lvert (h_{9/2})^2 i_{13/2}; {}^{29}/_{2}^{+}\rangle$	$\lvert f_{5/2}^{-1} i_{13/2}^{-1}; 7^{-}\rangle$	16.3	22.0	4455
$\lvert (h_{9/2})^2 i_{13/2}; {}^{29}/_{2}^{+}\rangle$	$\lvert f_{5/2}^{-1} i_{13/2}^{-1}; 8^{-}\rangle$	16.7	23.0	4556
$\lvert (h_{9/2})^2 i_{13/2}; {}^{29}/_{2}^{+}\rangle$	$\lvert f_{5/2}^{-1} i_{13/2}^{-1}; 9^{-}\rangle$	17.2	24.0	4580

In ^{201}At, the few lowest active proton shell-model orbitals are $h_{9/2}$, $f_{7/2}$, and $i_{13/2}$. Active neutron orbitals include hole excitations from the $i_{13/2}$ orbital. Such excitations may require a breaking of a neutron pair, but excitation energies of ~3–5 MeV are enough to make this energetically possible. All of these single-particle states have a high-j value, such as is required to form a shears band (property (iv)). In the inset of Fig. 10, the ^{204}At and ^{206}Fr backbending is astonishingly similar when compared to ^{201}At. This might suggest that the proton and neutron configurations in the shears bands of all these nuclei are similar. In the study by Hartley *et al.* [15] the proton and neutron configuration for ^{204}At and ^{206}Fr shears bands remained unknown. In these nuclei most likely the $h_{9/2}$ and/or $i_{13/2}$ proton states along with the $i_{13/2}$ neutrons are involved in the configuration of the shears bands [15].

For the band-head states in shears bands, the shears angle is $\sim 90^\circ$. Therefore, equation (1) can be used to calculate the band-head state spin in shears bands for different proton and neutron configurations. Similarly, by setting the shears angle to $\sim 0^\circ$, the maximum spin can be calculated. A selection of the results of such calculations is presented in Table V, together with the sum of proton- and neutron-state level energies. Corresponding experimental values are $^{23}/_{2}\ \hbar$ and 2990 keV for the band-head state, and $\sim 16\ \hbar$ and ~4200 keV for the observed band crossing. These experimental values match well with the calculated values shown in Table V, hence the proposed proton- and neutron-state configurations are $\pi(i_{13/2}) \otimes \nu(f_{5/2}^{-1} i_{13/2}^{-1}; 9^{-})$ for the lower cascade and $\pi((h_{9/2})^2 i_{13/2}) \otimes \nu(f_{5/2}^{-1} i_{13/2}^{-1}; 5^{-})$ above the band crossing. These configurations suggest a negative parity for the observed shears band. In several odd-mass lead isotopes

lighter than $A = 197$ a similar alignment have been observed (Ref. [46] and references therein). In these nuclei the band crossing is caused by the alignment of $i_{13/2}$ neutrons.

V. SUMMARY

In the present study of ^{201}At an isomeric $^{29}/_{2}^{+}$ state [$T_{1/2} = 3.39(9)$ μs] has been observed that is suggested to originate from the $\pi(h_{9/2}) \otimes {}^{200}\mathrm{Po}_{11^-}$ configuration. The isomer decays through the 269-keV $E2$ and 339-keV $E3$ transitions with reduced transition strengths of $1.33(4) \times 10^{-3}$ W.u. and 11(2) W.u., respectively. Some other observed excited states with their spins and single particle configurations are summarized in Table IV. We have also observed a cascade of magnetic dipole transitions that is suggested to form a shears band. The results of this study agree well with the previous results in the neighboring nuclei and the overall systematics in this region of the nuclide chart.

ACKNOWLEDGMENTS

This work has been supported by the Academy of Finland under the Finnish Center of Excellence Programme (2012-2017). The authors also thank the GAMMAPOOL European Spectroscopy Resource for the loan of the detectors for the JUROGAM II array. Support has also been provided by the EU 7th framework programme, Project No. 262010 (ENSAR). U.J. acknowledges support from the Finnish Academy of Science and Letters and the Vilho, Yrjö, and Kalle Väisälä Foundation.

[1] K. Heyde, P. van Isacker, M. Waroquier, J. L. Wood, and R. A. Meyer, Phys. Rep. **102**, 291 (1983).
[2] J. L. Wood, K. Heyde, W. Nazarewicz, M. Huyse, and P. van Duppen, Phys. Rep. **215**, 101 (1992).
[3] R. Julin, K. Helariutta, and M. Muikku, J. Phys. G: Nucl. Part. Phys. **27**, R109 (2001).
[4] K. Helariutta *et al.*, Eur. Phys. J. A **6**, 289 (1999).
[5] K. Van de Vel *et al.*, Eur. Phys. J. A **17**, 167 (2003).
[6] K. Dybdal, T. Chapuran, D. B. Fossan, W. F. Piel, D. Horn, and E. K. Warburton, Phys. Rev. C **28**, 1171 (1983).
[7] U. Jakobsson *et al.*, Phys. Rev. C **82**, 044302 (2010).
[8] R. F. Davie, A. R. Poletti, G. D. Dracoulis, A. P. Byrne, and C. Fahlander, Nucl. Phys. A **430**, 454 (1984).
[9] T. P. Sjoreen, G. Schatz, S. K. Bhattacherjee, B. A. Brown, D. B. Fossan, and P. M. S. Lesser, Phys. Rev. C **14**, 1023 (1976).
[10] I. Bergström, B. Fant, C. J. Herrlander, K. Wikström, and J. Blomqvist, Phys. Scr. **1**, 243 (1970).
[11] M. Nyman *et al.* Phys. Rev. C **88**, 054320 (2013).
[12] H. Kettunen *et al.*, Eur. Phys. A **17**, 537 (2003).
[13] R. M. Clark and A. O. Macchiavelli, Annu. Rev. Nucl. Part. Sci. **50**, 1 (2000).
[14] J. R. Novak *et al.*, Phys. Rev. C **59**, R2989 (1999).
[15] D. J. Hartley *et al.*, Phys. Rev. C **78**, 054319 (2008).
[16] R. M. Clark *et al.*, Phys. Rev. Lett. **82**, 3220 (1999).
[17] D. G. Jenkins *et al.*, Phys. Lett. B **428**, 23 (1998).
[18] A. Gadea *et al.*, Phys. Rev. C **55**, R1 (1997).
[19] F. Brandolini *et al.*, Phys. Lett. B **388**, 468 (1996).
[20] S. Frauendorf, Nucl. Phys. A **557**, 259c (1993).
[21] G. Duchêne *et al.*, Nucl. Instrum. Methods A **432**, 90 (1999)
[22] C. W. Beausang *et al.*, Nucl. Instrum. Methods A **313**, 37 (1992)
[23] C. Rossi Alvarez, Nucl. Phys. News **3**, 10 (1993)
[24] J. Sarén *et al.*, Nucl. Instrum. Methods A **654**, 508 (2011).
[25] M. Leino *et al.*, Nucl. Instrum. Methods B **99**, 653 (1995).
[26] R. D. Page *et al.*, Nucl. Instrum. Methods B **204**, 634 (2003).
[27] I. H. Lazarus *et al.*, IEEE Trans. Nucl. Sci. **48**, 567 (2001).
[28] P. Rahkila, Nucl. Instrum. Methods A **595**, 637 (2008).
[29] K. Auranen *et al.* Phys. Rev. C **90**, 024310 (2014).
[30] T. Kibédi *et al.*, Nucl. Instrum. Methods A **589**, 202 (2008).
[31] K. H. Schmidt, Eur. Phys. J. A **8**, 141 (2000).
[32] T. P. Sjoreen, U. Garg, and D. B. Fossan, Phys. Rev. C **23**, 272 (1981).
[33] L. A. Bernstein *et al.*, Phys. Rev. C **52**, 621 (1995).
[34] L. G. Mann *et al.*, Phys. Rev. C **38**, 74 (1988).
[35] K. Andgren *et al.*, Phys. Rev. C **78**, 044328 (2008).
[36] A. R. Poletti, G. D. Dracoulis, A. P. Byrne, A. E. Stuchbery, B. Fabricius, T. Kibèdi, and P. M. Davidson, Nucl. Phys. A **615**, 95 (1997).
[37] H. Beuscher, D. R. Zolnowski, D. R. Haenni, and T. T. Sugihara, Phys. Rev. Lett. **36**, 1128 (1976).
[38] A. M. Baxter, A. P. Byrne, G. D. Dracoulis, R. A. Bark, F. Riess, A. E. Stuchbery, M. C. Kruse, and A. R. Poletti, Nucl. Phys. A **515**, 493 (1990).
[39] T. P. Sjoreen, D. B. Fossan, U. Garg, A. Neskakis, A. R. Poletti, and E. K. Warburton, Phys. Rev. C **25**, 889 (1982).
[40] U. Jakobsson *et al.*, Phys. Rev. C **87**, 054320 (2013).
[41] U. Jakobsson *et al.*, Phys. Rev. C **85**, 014309 (2012).
[42] T. Wecström, B. Fant, T. Lönnroth, V. Rahkonen, A. Källberg, and C.-J. Herrlander, Z. Phys. A **321**, 231 (1985).
[43] A. Maj, H. Grawe, H. Kluge, A. Kuhnert, K. H. Maier, J. Recht, N. Roy, H. Hbel, and M. Guttormsen, Nucl. Phys. A **509**, 413 (1990).
[44] I. Bergström and B. Fant, Phys. Scr. **31**, 26 (1985).
[45] K. Honkanen, C. J. Herrlander, B. Fant, and T. Lönnroth, Nucl. Phys. A **451**, 141 (1986).
[46] A. Görgen *et al.*, Nucl. Phys. A **683**, 108 (2001).